Classical molecular-dynamics simulations of laser-irradiated clusters: Nonlinear electron dynamics and resonance-enhanced low-order harmonic generation

S. V. Fomichev* and D. F. Zaretsky†
Russian Research Center "Kurchatov Institute," Kurchatov place 1, 123182 Moscow, Russia and Max-Born-Institut, Max-Born Straße 2A, 12489 Berlin, Germany

D. Bauer‡ and W. Becker§
Max-Born-Institut, Max-Born Straße 2A, 12489 Berlin, Germany
(Received 2 September 2004; published 12 January 2005)

The nonlinear collective electron dynamics of a cluster irradiated by a strong near-infrared linearly polarized short laser pulse are studied by classical molecular-dynamics simulations for a small model cluster with $\sim 10^3$ particles. The model brings forth almost all of the features of a cluster exposed to a strong laser pulse, such as inner and outer ionization, expansion of the ion core, etc. When the frequency of the incident radiation is near three- or five-photon resonance with the (time-dependent) frequency of the dipole Mie-plasmon excitation in the laser-ionized and expanding cluster, both the total electron acceleration and the local electric field acting on the ions inside the cluster exhibit a resonant enhancement at the odd harmonics of the fundamental frequency. The time evolution during the laser pulse of these odd harmonics is discussed for different parameters of the laser-cluster interaction. The presence of even low-order harmonics (in particular, of the second) in the local electric field at ion positions off the cluster center is also demonstrated. This indicates nonlinear laser excitation of the quadrupole surface plasmon.

DOI: 10.1103/PhysRevA.71.013201 PACS number(s): 36.40.Gk, 36.40.Vz, 36.40.Wa, 42.65.Ky

I. INTRODUCTION

The interaction of subpicosecond near-infrared laser pulses with van der Waals and metal clusters has been extensively studied during the last decade. It has been demonstrated that atoms in clusters absorb energy from the laser field much more efficiently than isolated atoms [1–3]. Many other spectacular applications have been investigated, such as efficient x-ray emission [4–8], multicharged-ion production [9–11], and nuclear fusion in a medium of Coulomb-exploding clusters that contain deuterium [12,13]. In addition, efficient radiation of coherent high-order harmonics by laser-irradiated clusters of rare-gas atoms was observed [14,15]. In consequence, interest in laser-cluster interactions has enormously increased over the past years [16–18].

For clusters with radii between 2 and 20 nm (10^3–10^6 atoms), peak laser intensities in the range of 10^{15}–10^{17} W/cm^2, and pulse durations from several ten to several hundred femtoseconds, a sizable fraction of the electrons released by inner ionization does not leave immediately but stays inside the cluster during the duration of the laser pulse, in spite of the high ponderomotive energy of the electrons. These electrons are trapped by the net positive charge of the cluster as a whole, which has been built up by those electrons that did escape. As a result, a hot electron nanoplasma is created with unique properties [1]. The collective laser-driven motion of the electron cloud trapped inside the charged cluster and its immediate vicinity constitutes the important initial stage of the laser-induced cluster dynamics. Later on, Coulomb explosion of the positively charged ion background speeds up and finally turns the nanoplasmas of the individual clusters into one common high-temperature microplasma.

Linear excitation of the dipole surface (Mie) plasmon [19] by an intense laser pulse with frequency $\omega \approx \omega_{\mathrm{Mie}}$ constitutes a much-studied example of collective plasma phenomena in finite systems [20]. It has been extensively investigated, both in metal clusters [21–23] and in laser-ionized rare-gas atomic clusters [1,3]. This well-known Mie resonance corresponds to a rigid oscillation of the cloud of free electrons in the cluster with respect to the background of the positively charged ions. For spherical clusters, it occurs at the frequency

$$\omega_{\mathrm{Mie}} = \sqrt{4\pi e^2 n/3m_e} \equiv \omega_{\mathrm{p}}/\sqrt{3}, \tag{1}$$

where m_e and e are the electron mass and charge, respectively, $n = zN_i/V$ the (mean) positive (ion) charge density inside the cluster, N_i the total number of atoms and ions, and z their mean charge state averaged over the whole cluster volume V. In the resonant regime, which requires $n \approx 3n_{\mathrm{cr}}(\omega) \equiv 3\omega^2 m_e/4\pi e^2$, efficient excitation of the Mie resonance can result in a considerable enhancement of the cluster's inner electric field at the fundamental frequency. This, in turn, may significantly influence the heating of the electron nanoplasma, the multiple ionization of the atoms and ions inside the cluster, and other laser-induced processes. However, linear excitation of the Mie resonance by a near-infrared laser ($n_{\mathrm{cr}} \approx 1.7 \times 10^{21}$ cm^{-3} for a Ti:sapphire laser) requires the density n to be much lower than it really is just after inner ionization of the cluster (when we have $\omega_{\mathrm{Mie}} \sim 4$–$6$ eV for $n \sim 10^{22}$–10^{23} cm^{-3}).

*Electronic address: fomichev@imp.kiae.ru
†Electronic address: zaretsky@imp.kiae.ru
‡Electronic address: dieter.bauer@mpi-hd.mpg.de
§Electronic address: wbecker@mbi-berlin.de

 ©2005 The American Physical Society

TABLE I. Mie-resonance wavelengths λ_{Mie} (in nanometers) from Eq. (1) for rare-gas atomic clusters with mean charge state Z, where the cluster constituents are packed into an fcc lattice having the solid-phase lattice constant d_0, as well as the corresponding appearance intensities I_{app} (in $\mathrm{W/cm^2}$) for over-the-barrier ionization of isolated rare-gas ions in vacuum.

fcc lattice parameter[a] d_0 (nm)	Ne 0.446		Ar 0.526		Kr 0.572		Xe 0.620	
	λ_{Mie}	I_{app}	λ_{Mie}	I_{app}	λ_{Mie}	I_{app}	λ_{Mie}	I_{app}
$Z=1$	268	8.7×10^{14}	343	2.5×10^{14}	389	1.5×10^{14}	439	8.7×10^{13}
$Z=2$	189	2.8×10^{15}	243	5.8×10^{14}	275	3.5×10^{14}	317	1.9×10^{14}
$Z=3$	155	7.2×10^{15}	198	1.2×10^{15}	225	8.3×10^{14}	254	4.1×10^{14}
$Z=4$	134	2.2×10^{16}	172	3.2×10^{15}	195	1.9×10^{15}	220	1.0×10^{15}
$Z=5$	120	4.1×10^{16}	154	5.1×10^{15}	174	2.9×10^{15}	197	2.0×10^{15}
$Z=6$	110	6.9×10^{16}	141	7.6×10^{15}	159	4.2×10^{15}	180	3.0×10^{15}

[a]From Ref. [24]. Note that the rare-gas elements in the low-temperature solid phase crystallize into an fcc structure.

Therefore, efficient *one-photon* excitation of the Mie resonance can only be expected in the two transient regimes when the ion density is sufficiently reduced: during the Coulomb-explosion stage of the heated charged cluster (reduced N_i/V, provided this stage is reached while the laser pulse is still on) or, in principle, during the leading edge of the laser pulse, when the time-dependent laser intensity and, consequently, the degree of ionization of the cluster constituents are still low (since z is low). For clusters consisting of rare-gas atoms, these statements are substantiated in Table I, where the reference Mie-resonance wavelength λ_{Mie} (which is typically much lower than 800 nm) is given for different (mean) charge states of the cluster ions. They were calculated under the assumption that the cluster atoms and ions are packed into a face-centered-cubic (fcc) lattice with the lattice constant d_0 corresponding to the low-temperature solid phase of rare-gas elements [24]. The critical intensities for the appearance of the various charge states Z of isolated rare-gas ions by over-the-barrier ionization in vacuum [25], $I_{\mathrm{app}}=c(I_p^Z)^4/(128\pi e^6 Z^2)$, are also given ($I_p^Z$, taken from Ref. [26], is the ionization potential of an ion with charge state $Z-1$ and c is the speed of light).

Nonlinear (multiphoton) excitation of the dipole Mie resonance in jellium clusters in the weak-field regime has recently been considered [27]. Excitation of higher-order multipole plasmons, with the frequencies

$$\omega_l = \sqrt{4\pi e^2 nl/[(2l+1)m_e]} \equiv \omega_{\mathrm{p}}\sqrt{l/(2l+1)} \quad (l=1,2,\ldots) \tag{2}$$

in the spherical case, is also considered in this paper. Indeed, quasiresonant three-photon excitation of the *dipole* Mie plasmon ($l=1$) by a Ti:sapphire laser ($\lambda/3\approx266$ nm) in laser-irradiated rare-gas clusters appears to be possible for several cases presented in Table I, as long as the mean ion charge is not too high. If, on the other hand, the mean ion charge is higher than 3, three-photon excitation of the Mie resonance may be realized in the transient regimes—namely, during the leading edge of the laser pulse and again during the Coulomb-expansion stage of the charged cluster, as mentioned above. Moreover, in this case a five-photon quasiresonant excitation of the dipole Mie plasmon is also possible. For all but a few of the examples presented in Table I (those in the upper right), the conditions for three-photon excitation of the Mie resonance are actually met at least transiently. In the Coulomb-expansion stage, this always takes place prior to the linear (one-photon) Mie-resonance excitation, because the latter requires a lower positive charge density, which is reached at a later time.

Nonlinear excitation of the Mie resonance in strong laser fields has been discussed only recently. Within a *macroscopic* approach, three-photon excitation of the Mie resonance in a laser-irradiated large cluster has been investigated in Refs. [28–30]. This study was based on the simplest approximation to the hydrodynamic equations, which treats the electrons trapped by the cluster as an incompressible fluid having the quasiequilibrium electron density. In this approximation, under the action of a strong laser pulse the electron cloud oscillates without deformation. In general, this approximation is justified only if the oscillation amplitude of the electron cloud is much smaller than the cluster radius. The motion of the ions was neglected, assuming pulses short enough that the expansion of the cluster had just only started at the end of the pulse. Near three-photon resonance with the Mie frequency (at $3\omega\approx\omega_{\mathrm{Mie}}$), the electric field inside the cluster was found to have a third-harmonic component, with a magnitude comparable with that at the fundamental frequency inside the cluster. Due to shielding, the latter is, in general, smaller than the amplitude of the incident laser field in this parameter range of an overcritical charge density. The third harmonic is also present and resonantly enhanced in the scattered electromagnetic field. The physical origin of the high conversion efficiency from the fundamental into the third harmonic is the finite size of the cluster. In the perturbation series with respect to the ratio of the oscillation amplitude of the electron cloud to the cluster radius, this provides the nonlinear terms in the restoring force of the electron-ion interaction, beginning with the cubic term [31,32].

Recent pump-probe experiments in laser-irradiated argon clusters actually provided first evidence of the enhancement of third-harmonic generation by three-photon excitation of the Mie resonance [33]. In parallel, a model particle-in-cell simulation showed the presence of the third harmonic in the electron acceleration [34,35]. Also, in very recent micro-

scopic particle-in-cell (MPIC) simulations of large laser-irradiated clusters with $\sim 10^5$ atoms [36], a nonlinear contribution to the cluster's electron current is clearly visible though not discussed.

However, within the macroscopic approach based on the hydrodynamic equations, the width of the linear Mie resonance in the laser-heated charged cluster can only be introduced phenomenologically. Generally, it is determined both by electron-ion collisions and by the irreversible part of Landau damping in a finite system. In addition, the possibility of nonlinear laser excitation of multipole plasmon modes other than the dipole (e.g., the quadrupole plasmon that corresponds to $l=2$) is beyond the approximation of the rigid electron cloud. Moreover, the time dependence of the Mie frequency, which results from the expansion of the charged cluster during the action of the laser pulse, is outside of the simplest macroscopic approach. Hence, even though the physical picture obtained is clear, only a semiquantitative description of the nonlinear excitation of the dipole Mie plasmon in the laser-irradiated cluster can be achieved within the approximations of Refs. [28–30].

The aim of the present work is to study the nonlinear electron dynamics inside a laser-irradiated cluster by means of a classical molecular-dynamics simulation of a small cluster consisting of $\lesssim 10^3$ atoms. Previous classical simulations of small clusters [37–45] were predominantly concerned with the dynamics of the Coulomb explosion. The goal of the present *microscopic ab initio* study is to confirm the presence of the third harmonic (and of higher harmonics, too) in the electron acceleration as well as in the local electric field acting on the ions inside the cluster, while the frequency of the incident laser sweeps through the corresponding nonlinear resonance with the Mie frequency. Obviously, for a spherical cluster, only odd harmonics should be expected in the total electron acceleration (that is, the sum of the acceleration of all electrons), as well as in the local electric field at the center of the cluster. Even-order harmonics of the fundamental frequency can be expected in the local electric field acting on ions at noncentral positions. Indeed, we will demonstrate their presence, in particular, the second harmonic, which is connected with the quadrupole surface-plasmon excitation.

Preliminary results have already been presented in Ref. [46], where a cluster of two-electron model atoms was considered. It was shown that under appropriate conditions the laser-driven nonlinear oscillation of the electron cloud generates a resonantly enhanced third harmonic both in the total electron acceleration and in the inner electric field. The time-dependent yield of the third harmonic was analyzed for different parameters of the laser-cluster interaction, and the resonance behavior of the third harmonic excitation was investigated. In this paper, we extend our model to cluster atoms having more than two electrons. We allow sequential ionization of atoms and ions inside the cluster under the action of the inner electric field, which is the superposition of the laser field, the alternating electric field generated by the collective electron motion, and the quasistatic electric field of the ions, as considered in the ionization ignition model [47,48]. Apart from the restriction to a maximal ionic charge state, this is close to the realistic case of a rare-gas atomic cluster in a strong laser field.

The paper is organized as follows. The simulation model employed is described in Sec. II, and its results are presented in Sec. III. Results for the benchmark case of a small argon-like cluster with 675 atoms with a maximal ion charge state $Z_{\max}=2$ are shown in Sec. III A. These results supplement those obtained earlier [46]. In Sec. III B, we reconsider the argonlike cluster with 675 atoms, allowing for the higher maximal charge state $Z_{\max}=4$. We also investigate a xenon-like cluster with 459 atoms and with $Z_{\max}=6$. Specifically, the properties of the low-order odd harmonics, including their temporal profile and their resonance behavior, are discussed in Sec. III B 1, and the even harmonics, in particular the second, in the inner electric field off the center of the cluster are inspected in Sec. III B 2. Concluding remarks terminate the paper in Sec. IV.

II. SIMULATION MODEL

The simulations were performed for a small model cluster consisting of $N_i \lesssim 10^3$ neutral atoms of mass M_i corresponding to argon or xenon (40 or 130 amu, respectively) with discrete spherical symmetry in its initial state. Before the action of the laser pulse, the atoms are packed into a fcc lattice surrounded by a sphere with its center at the (0,0,0) atom position of the fcc lattice. We utilize this structure, which is observed for rare-gas elements in their solid phase, instead of the Mackay icosahedra structure, which is typical for small Lennard-Jones clusters [49], assuming that the nonlinear phenomena under investigation are rather insensitive to the detailed arrangement of the atoms in the cluster, but not to the cluster density. The radius was chosen such that the surrounding sphere contains exactly N_i atoms (675 for our argonlike cluster and 459 for the xenonlike cluster). The interatomic distance along the main axes of the cluster's fcc structure (the lattice constant d_0) was taken as 0.526 nm for the argon cluster and 0.620 nm for the xenon cluster (cf. Table I), which leads to an initial cluster radius R_0 of about 1.8 nm.

As is typically done in such simulations, the electrostatic interaction between any pair of charged particles in the cluster is modeled by a smoothed Coulomb potential $\sim(r^2+a^2)^{-1/2}$ with the smoothing parameter $a=0.09$ nm for argon or $a=0.12$ nm for xenon. These values are chosen such that the minimum of the electron-ion interaction potential agrees with the ionization potential I_p^1 of the neutral atom—that is, such that $e^2/a=I_p^1$. At the beginning of the calculations, one electron is assigned to each cluster atom, which is placed with zero kinetic energy at the bottom of its binding potential, in order to mimic the neutral atom. Once this first electron has become free under the action of the applied electromagnetic field, the ion charge is changed from $Z=1$ to $Z=2$ and an additional electron is put into a bound state of the respective ion with binding energy $I_p^2=2e^2/a$, and so on. (Note that the actual ionization potentials I_p^Z of rare-gas ions are approximately proportional to Z up to $Z=6$; cf. Ref. [26].) In this process, we consider an electron as free when it has reached a distance of $0.7d_0$ from its parent ion. We checked that the results are not very sensitive to the actual choice of this distance. The maximal charge state that can be

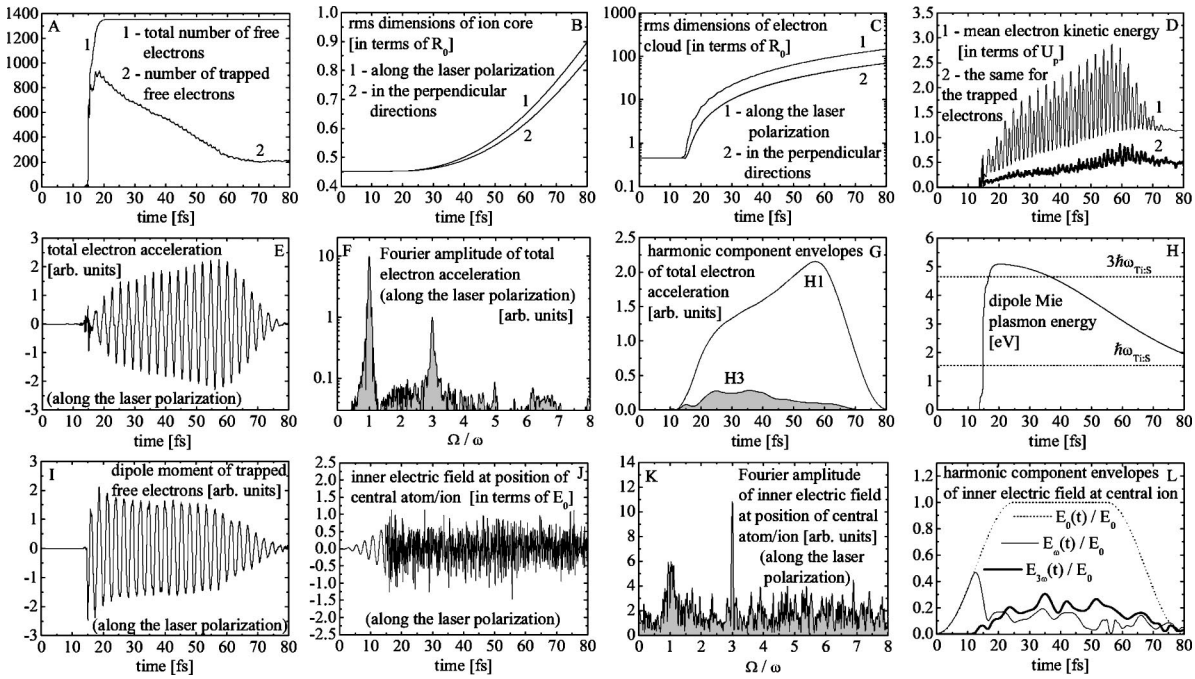

FIG. 1. As indicated on each panel, panels (A)–(L) exhibit various nonlinear features for a small (675 atoms) model argon cluster with $Z_{max}=2$ exposed to a 80 fs laser pulse ($\lambda=800$ nm, $I_0=2\times10^{15}$ W/cm^2).

reached this way by each ion is restricted to $Z_{max}=2$ or $Z_{max}=4$ for our argon cluster and to $Z_{max}=6$ for our xenon cluster. These values seem to be reasonable (especially if shielding is taken into account) in view of the corresponding appearance intensities I_{app} presented in Table I for the range of laser intensities that we consider.

The motion of each individual charged particle (electron or ion) participating in the cluster dynamics is due to the combined action of the external laser field and the total field of all of the other charged particles. The calculations were performed for a linearly polarized laser pulse with peak intensity $I_0=cE_0^2/8\pi$ in the range of some petawatt per centimeter square (1 PW/cm$^2\equiv10^{15}$ W/cm^2) and a total duration of $T=80$ fs, which is turned on and off according to

$$E(t)=E_0\times\begin{cases}\sin^2(\pi t/2T_1)\cos\omega t,\\ \cos\omega t,\\ \sin^2(\pi(T-t)/2T_1)\cos\omega t,\end{cases}\qquad(3)$$

for $0\leqslant t\leqslant T_1$, $T_1\leqslant t\leqslant T-T_1$, and $T-T_1\leqslant t\leqslant T$, respectively, with $T_1=25$ fs. Newton's equations of motion for each of the charged particles were solved using a code based on the Verlet algorithm in the velocity form [50], with a time step of 5 as.

We calculate the total electron acceleration (that is, the sum of the accelerations of all electrons) and the local electric field that acts on those particular ions that were initially placed at the position (0,0,0) at the cluster center, and at (2,0,0), (0,2,0), and (0,0,2) away from the center along each of the three cubic axes. This distance is approximately half the cluster radius. For the systematic investigation of the properties of the third (and also fifth, if present) harmonic, the polarization of the laser field was taken at some moderate angle with respect to the z axis of the fcc lattice. Calculations were also performed with the laser-field polarization exactly along the z axis. This makes it possible to control the symmetry properties of the local inner electric field. It turned out that the amplitudes of the harmonics in the electron acceleration are largely independent of the direction of the incident laser field.

III. RESULTS OF THE SIMULATIONS

A. Argonlike cluster with 675 atoms and $Z_{max}=2$

As a starting point of our study, we present the results of calculations for an argonlike model cluster with 675 atoms when the maximal ion charge is restricted to $Z_{max}=2$. For the laser wavelength $\lambda=800$ nm, we compare in Figs. 1 and 2 various nonlinear features of the electron dynamics for peak intensities of $I_0=2\times10^{15}$ and 4×10^{15} W/cm^2, respectively. Panels (A)–(L) of Figs. 1 and 2 then present the basic nonlinear features of the electron dynamics caused by the laser-cluster interaction. The panels display, as functions of time during the 80-fs laser pulse, the total number of free electrons released by inner ionization as well as of the fraction that stays trapped inside the cluster (A), the root-mean-square dimensions of the cluster's ion core (B) and the electron cloud (C) both parallel and perpendicular to the laser polarization, the mean kinetic energy of all electrons and of the part that is trapped (D), and the total electron acceleration (E) along the laser polarization.

As time goes on, the electron cloud builds up as electrons under the action of the laser pulse leave their initial bound states, as soon as the local electric field reaches the critical value for the classical over-the-barrier ionization process [25]. For our parameters, inner ionization starts between 10 and 20 fs after arrival of the pulse and is complete after

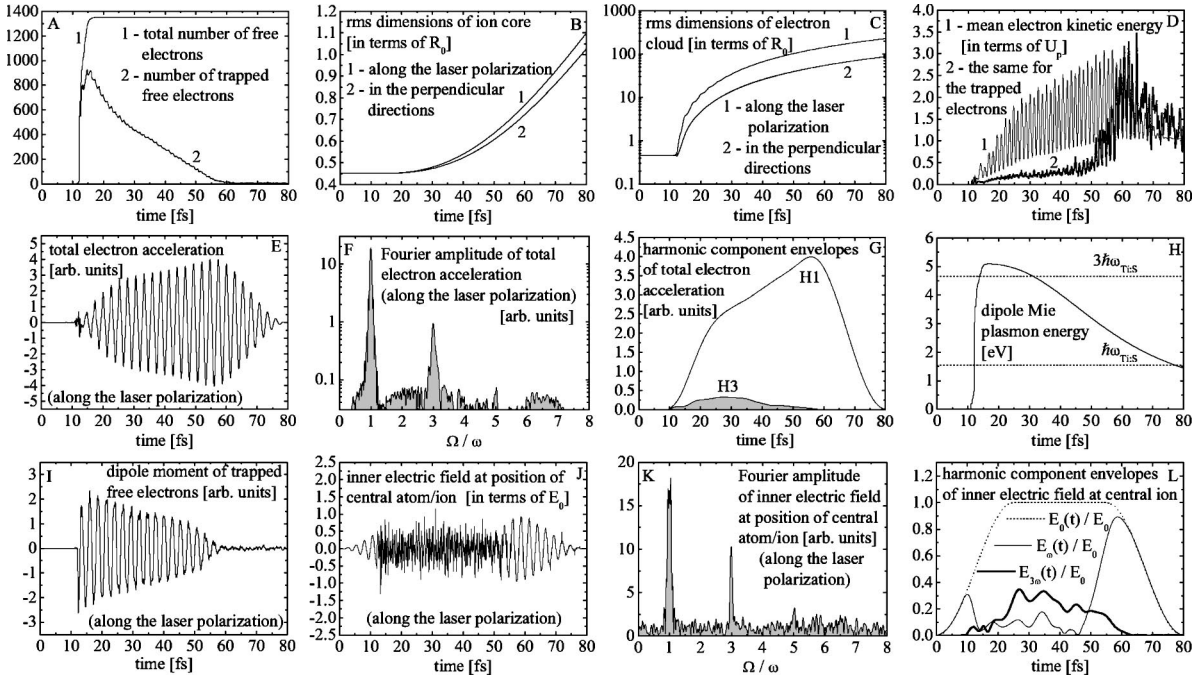

FIG. 2. Same as in Fig. 1, but for the higher laser intensity $I_0 = 4\times10^{15}$ W/cm^2.

$\approx$20 fs when all the electrons have left their parent atoms or ions. For an 80-fs laser pulse with peak intensity $I_0 = 4\times10^{15}$ W/cm^2, at the end of the pulse practically all of the electrons have escaped from the cluster to positions far away [Fig. 2(A)], leading to almost complete outer ionization of the cluster. On the other hand, if the intensity is reduced to 2×10^{15} W/cm^2, a substantial fraction of the electrons remains trapped inside [Fig. 1(A)]. The number of electrons either inside the cluster or closely outside of it depends on time and on the laser intensity. It is calculated as the number of electrons inside a sphere of twice the root-mean-square radius of the expanding (axially symmetric) ion core, extracted from the data presented in Fig. 1(B) or 2(B). [The slight deviation from spherical symmetry of the expanding ion core is induced by the more pronounced laser-induced axial symmetry of the electron cloud; cf. Figs. 1(C) and 2(C).] It is these electrons that are responsible for the nonlinear effects under consideration. Their mean kinetic energy $\varepsilon_e^{\text{trapped}} \lesssim 0.5U_p$ is generally much lower than the ponderomotive potential $U_p = e^2E_0^2/4m_e\omega^2$ of the incident laser field; cf. curves 2 in Figs. 1(D) and 2(D).

Due to the expansion of the ion core, the Mie-plasmon energy $\hbar\omega_{\text{Mie}}$ [Eq. (1)] is also time dependent: ignoring the slight deviation of the expanding ion core from spherical symmetry, Figs. 1(H) and 2(H) demonstrate that $\hbar\omega_{\text{Mie}}(t)$ reaches its maximum around the time when inner ionization just becomes complete. Near its maximum, it slightly exceeds the total energy of three Ti:sapphire laser photons. Subsequently, it slowly decreases as Coulomb explosion sets in. For the conditions of Fig. 2, the few electrons that remain trapped inside the cluster up to the end of the pulse [Fig. 2(A)] cannot efficiently shield the incident laser field and, besides, the ion density is reduced so that linear resonance with the Mie frequency becomes possible [Fig. 2(H)]. This results in a considerable enhancement of the mean kinetic energy of these few trapped electrons near the end of the pulse, as can be seen in Fig. 2(D).

The properties of the third harmonic of the total electron acceleration along the laser polarization are shown in Figs. 1(F), 1(G), 2(F), and 2(G). The presence of harmonics is already visible in the time dependence of the total electron acceleration $a(t)$ [Figs. 1(E) and 2(E)], as well as in the dipole moment of the trapped electrons [Figs. 1(I) and 2(I)], notably during the first half of the pulse. In the semilogarithmic plots of the amplitude $|\tilde{a}(\Omega)|$ of the Fourier transform (FT) of the electron acceleration over the entire pulse length, $\tilde{a}(\Omega) = \int_0^T a(t)e^{i\Omega t}dt$ [Figs. 1(F) and 2(F)], the third harmonic peak is very conspicuous. Comparison of the plots for the two laser intensities 2×10^{15} and 4×10^{15} W/cm^2 shows that the intensity dependence of the third harmonic is weak and has nothing to do with the conventional cubic law implied by lowest-order perturbation theory. Obviously, in our case of a small cluster perturbation theory is inapplicable, because the oscillation amplitude of the electrons is not small compared with the cluster radius. For a small cluster, the residual intensity dependence is mainly related to the strong reduction of the number of trapped electrons as the laser intensity increases. Figures 1(G) and 2(G) show the time profile $a_{3\omega}(t)$ of the third-harmonic component of the electron acceleration. They confirm the correlation with the time-dependent number of trapped electrons [Figs. 1(A) and 2(A)]. All time profiles of nth-order harmonic components ($n \geqslant 1$) were calculated from the Fourier transform as

$$a_{n\omega}(t) = 2\left|\int_{-\Omega_1}^{\Omega_1} \tilde{a}(\Omega + n\omega)W_{\text{H}}(\Omega)e^{-i\Omega t}\frac{d\Omega}{2\pi}\right|, \qquad (4)$$

where $W_{\text{H}}(\Omega) = 0.5[1+\cos(\pi\Omega/\Omega_1)]$ is the Hanning window, which extends from $-\Omega_1$ to Ω_1. In our calculations we used $\Omega_1 = 0.75\omega$.

Figures 1(J)–1(L) and 2(J)–2(L) illustrate the temporal properties of the inner electric field acting on the ion that is initially positioned at the lattice point (0,0,0) at the center of the cluster. The FT amplitudes of the field component along the laser polarization are shown for the intensities $I_0=2\times10^{15}$ and 4×10^{15} W/cm^2, respectively, in Figs. 1(K) and 2(K). For the low intensity, the third harmonic is the strongest component of the field. Due to shielding, the field at the fundamental frequency at the center of the cluster is strongly reduced with respect to the incident field. Figure 1(L) shows that the third harmonic successfully competes with the fundamental throughout the entire length of the laser pulse. However, it should be noticed that for the low intensity the third harmonic is present on top of a very pronounced noisy background, which is mainly due to quasifree electrons that are temporarily trapped by ions. The effect of this "classical recombination" is reduced with increasing laser intensity and finally becomes entirely insignificant. As a consequence, for the higher intensity of $I_0=4\times10^{15}$ W/cm^2 the background noise is much lower. During the first half of the laser pulse, Fig. 2(L) is very similar to Fig. 1(L) at the lower intensity. Later, however, when almost all electrons have left the cluster [cf. Fig. 2(A)] the inner field at the fundamental frequency actually coincides with the incident laser field, and the third harmonic field has completely disappeared.

Figures 1(H) and 2(H) show that, for the argon cluster with $Z_{\max}=2$ and the laser wavelength of 800 nm, during a significant fraction of the pulse the nominal time-dependent Mie frequency (1) near its maximum is close to three-photon resonance with the incident frequency. Since the temporal profile of the Mie frequency only weakly depends on the laser wavelength, the conditions for resonance can be varied by simply varying the latter. Figure 3(A) shows that for $\lambda \lesssim 725$ nm the condition for three-photon resonance is nowhere met during the pulse duration, while for $\lambda \gtrsim 725$ nm there are two times t such that $3\omega=\omega_{\mathrm{Mie}}(t)$. This is reminiscent of the quantum-mechanical Landau-Zener level-crossing problem [51–53], where the detuning from resonance also depends on time and gradually passes through resonance. With decreasing laser wavelength, the two resonance times approach each other until, at some critical wavelength, they coincide. This situation is physically quite similar to the case of parabolic level crossing [54]. Excitation of the third harmonic is expected to be most efficient near this critical wavelength. Indeed, this is borne out by Fig. 3(B), which plots the total energy emitted into the third harmonic—viz., the quantity $\int_0^T a_{3\omega}^2(t)dt$—as a function of the laser wavelength, for the two intensities of 2×10^{15} and 4×10^{15} W/cm^2. Both curves exhibit typical resonance behavior centered at wavelengths slightly below 800 nm, which is redshifted by about 10% from the critical wavelength of 725 nm; cf. Fig. 3(A).

Such a redshift of the effective Mie frequency in a cluster in an intense field is not surprising and has been noted before [28–30]. This shift can be induced by nonlinear terms in the interaction of the electrons with the ion background, and in this case it could be intensity dependent (at least if perturbation theory were applicable). On the other hand, it is well known that a redshift of the effective Mie frequency with respect to its nominal position already exists in small cold

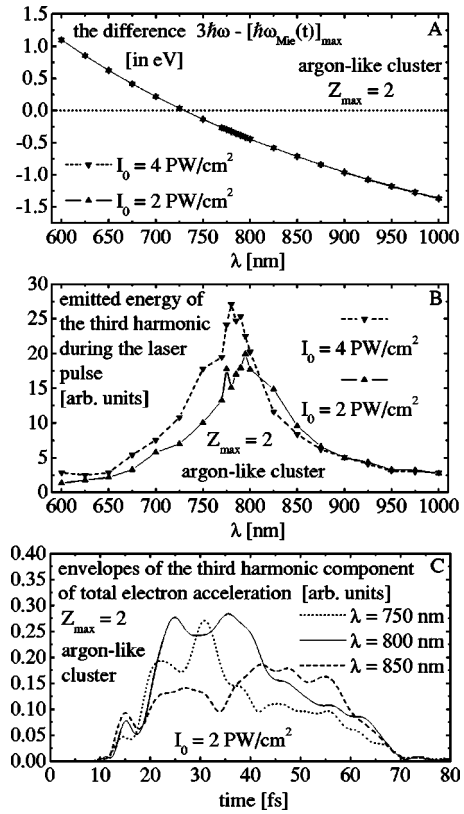

FIG. 3. For the conditions of Figs. 1 and 2, the panels show (A) the detuning (in eV) between three times the laser-photon energy and the maximal value of the nominal time-dependent Mie-plasmon energy (1) versus the laser wavelength, (B) the resonance curves of the third-harmonic yield for two laser intensities $I_0=2\times10^{15}$ and 4×10^{15} W/cm^2, and (C) the time-dependent envelopes of the third harmonic of the total electron acceleration for three different wavelengths and $I_0=2\times10^{15}$ W/cm^2.

metal clusters in the weak-field regime [55,56]. In this case, it is determined by spill-out of the electron cloud beyond the boundary of the positive background due to tunneling or over-the-barrier ionization. This creates an electron halo around the cluster. In our case of a small cluster in a strong laser field, we expect both effects to contribute. In our calculations of the resonance curve, we cannot separate them, but we can check the intensity dependence of the effective Mie frequency comparing the resonance curves for two laser intensities. The results presented in Fig. 3(B) show that, in our case of a small cluster, the redshift of the Mie-frequency is practically independent of the laser intensity, again indicating the inapplicability of perturbation theory in our parameter range.

Notice also the double-peak shape of the resonance curve, which is present for both laser intensities. We have observed such a structure before [46], and it appears to be typical. Figure 3(C) displays the time-dependent envelopes of the third-harmonic component of the total electron acceleration at and on either side of the resonant wavelength—namely, at 800, 750, and 850 nm, respectively. They clearly display the general trend expected on the basis of the picture sketched thus far: For short wavelengths, third harmonic generation is strongest around the time t when $\omega_{\mathrm{Mie}}(t)$ comes closest to

3ω. As the laser wavelength increases, the third-harmonic envelope develops two maxima at times that correspond qualitatively, though not quantitatively, to the times t when nominal resonance occurs—namely, when $3\omega=\omega_{\mathrm{Mie}}(t)$. Interference of the third harmonic emitted at these two times may explain the double-peak resonance observed in Fig. 3(B).

The width of the resonance in Fig. 3(B) [full width at half maximum (FWHM)] of about 100 nm is practically the same for the two laser intensities considered. Corresponding to ≈ 0.2 eV, it is rather small, on the scale of the electron-ion collision frequency $\nu_{\mathrm{ei}} \sim 4\pi z n e^4 L / m_e^2 v_e^3$ as well as of the Landau-damping frequency $\nu_{\mathrm{Ld}} \sim v_e / R$ [57], where L denotes the Coulomb logarithm, $v_e = (2\varepsilon_e^{\mathrm{trapped}}/m_e)^{1/2}$ a typical velocity of the trapped electrons (the quiver or the thermal velocity whichever is higher), and R the cluster radius. Both frequencies are of the order of at least 1 eV. The low value of the width, which resulted from our calculations, supports the conclusion arrived at earlier on the basis of classical simulations [36,40,41]: the properties of laser-irradiated clusters are not dominated by individual electron-ion collisions in the wavelength regime that is here considered. The small width that we found is, however, well compatible with the mechanism of Landau damping (collisions of the electrons with the cluster boundary created by the ion background): one just has to take into account that, for our case of a small cluster in an intense field, the electrons oscillate with an amplitude that significantly exceeds or at least is comparable with the cluster radius R (if shielding of the inner electric field is taken into account). Moreover, in contrast to the case of cold clusters in the weak-field regime, the electrons accelerated by the strong laser field are not perfectly reflected by the inner cluster surface (nor by the outer). They can penetrate the cluster surface and return later, driven by the intense laser field, with absorption of laser energy by the vacuum-heating mechanism [58,59]. Compared with the simple reference estimate given above, this can significantly reduce the rate of the irreversible part of Landau damping, which is connected with the interaction of the electrons with the potential of the ion background as a whole, in accordance with our findings.

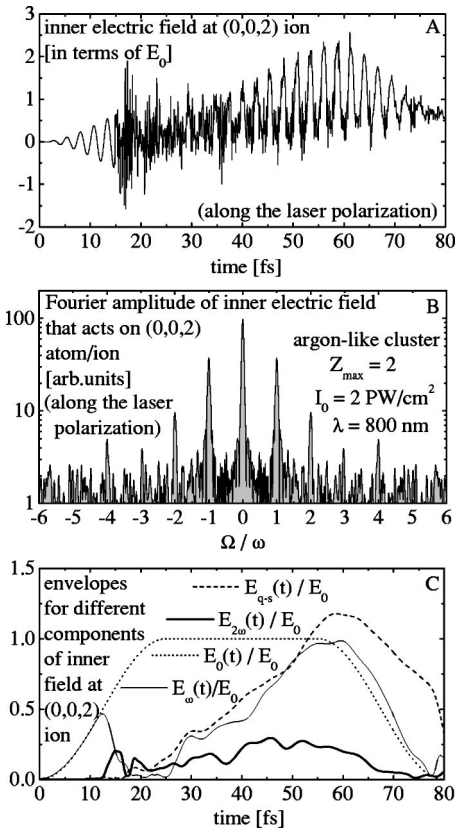

FIG. 4. For the conditions of Fig. 1, the panels show (A) the inner electric field along the laser polarization at the instantaneous positions of the (0,0,2) ion, (B) its Fourier spectrum, and (C) the time-dependent envelopes of several harmonic components of this field [including its quasistatic component, $E_{q-s}(t)$].

Figure 4(A) exhibits the inner electric field that acts on the ion whose initial position was at the lattice point (0,0,2) off the center of the cluster along the z axis—that is, in this case, in the direction of the laser polarization. By far the strongest component of its Fourier transform is the quasistatic component [Fig. 4(B)]. It is caused by the ion distribution, which is not symmetric with respect to the positions of this *moving ion*. Figure 4(C) confirms this picture: After

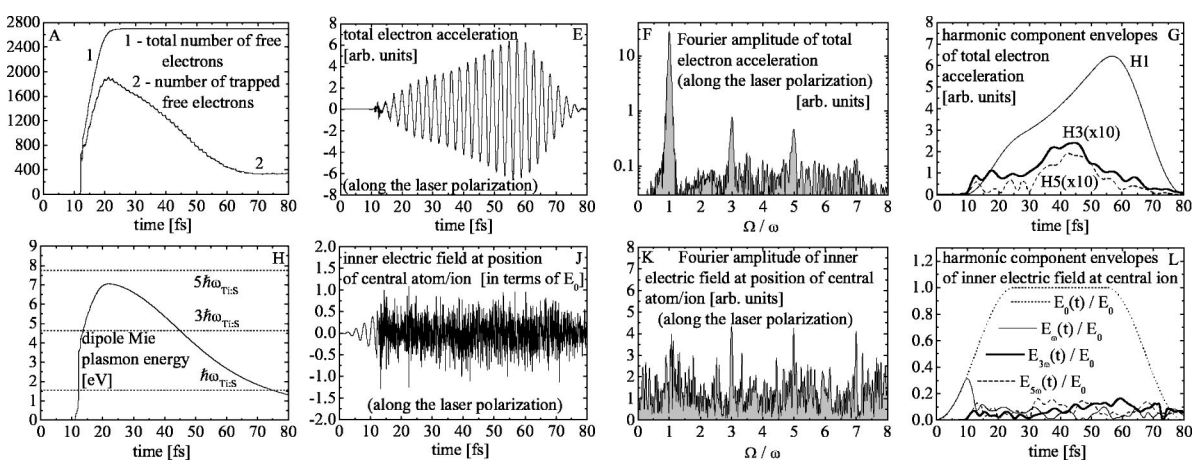

FIG. 5. As indicated on each panel, the panels show the nonlinear features of the laser-cluster interaction for a small (675 atoms) model argon cluster with $Z_{\max}=4$ exposed to a 80-fs laser pulse ($\lambda=800$ nm, $I_0=4\times10^{15}$ W/cm^2.

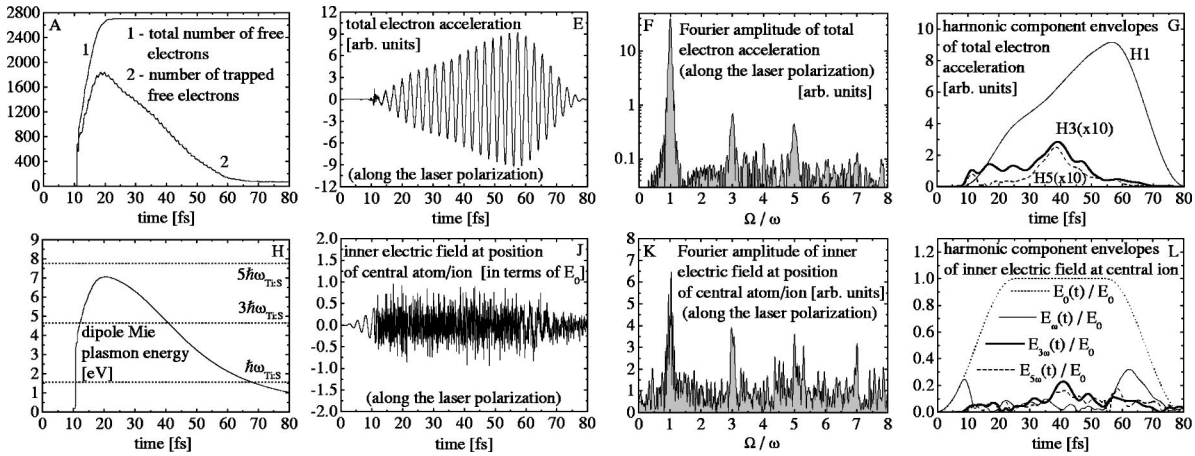

FIG. 6. Same as in Fig. 5, but for the higher laser intensity $I_0 = 6\times 10^{15}$ W/cm^2.

inner ionization is almost complete, the quasistatic component keeps rising in pace with the decreasing number of trapped electron [cf. Fig. 1(A)]. At the end of the pulse, the remaining trapped electrons rearrange themselves into the most symmetrical configuration, and the quasistatic component drops to a smaller value.

The next-strongest component is the fundamental, followed by the second harmonic. The presence of the latter indicates excitation of nondipole (e.g., quadrupole) plasmons, which cannot be described in terms of oscillations of a rigid electron cloud without deformations. The temporal resonance condition for the excitation of the second harmonic, $2\hbar\omega = \hbar\omega_{l=2}(t) = \sqrt{6/5}\hbar\omega_{\mathrm{Mie}}(t)$ [cf. Eq. (2), in terms of the nominal Mie frequency (1)], is satisfied in the beginning and at the end of the laser pulse for a much wider range of wavelengths than for the third harmonic. A more comprehensive study of second-harmonic excitation is presented below in Sec. III B 2 for the example of a xenon cluster with 459 atoms and $Z_{\max} = 6$. Moreover, owing to the restriction in this section of each cluster atom to two electrons, it was not possible to explore how continuing inner ionization of the cluster by the *inner* electric field would affect the harmonics at high laser intensity. This question is further discussed below.

B. 675-atom model argon cluster with $Z_{\max} = 4$ and 459-atom model xenon cluster with $Z_{\max} = 6$

1. Odd-harmonic generation

Similarly to Figs. 1 and 2 of the previous Sec. III A, the results of simulations that allow for more than two electrons per atom are presented in Figs. 5 and 6 for a 675-atom model argon cluster with $Z_{\max} = 4$ and in Figs. 7 and 8 for a 459-atom model xenon cluster with $Z_{\max} = 6$. The two sets of figures for each case correspond to the two laser intensities of 4×10^{15} and 6×10^{15} W/cm^2, respectively. For each particular case, we present only those properties that are most relevant to harmonic excitation. (The results for the expansion of the ion core and the electron cloud, as well as for the mean kinetic energy of the electrons, are not shown since they are very similar to those presented in Figs. 1 and 2 for the two-electron-atom case.) As can be seen from Figs. 5–8, *most* of the features of the laser-cluster interaction in these cases are qualitatively similar to the case of the two-electron atom. The main effect caused by the presence of more electrons per atom is the appearance of the fifth harmonic with a strength comparable with the third in the total electron acceleration [panels (F)] and in the inner electric field at the position of the central cluster ion [panels (K)]. The seventh harmonic

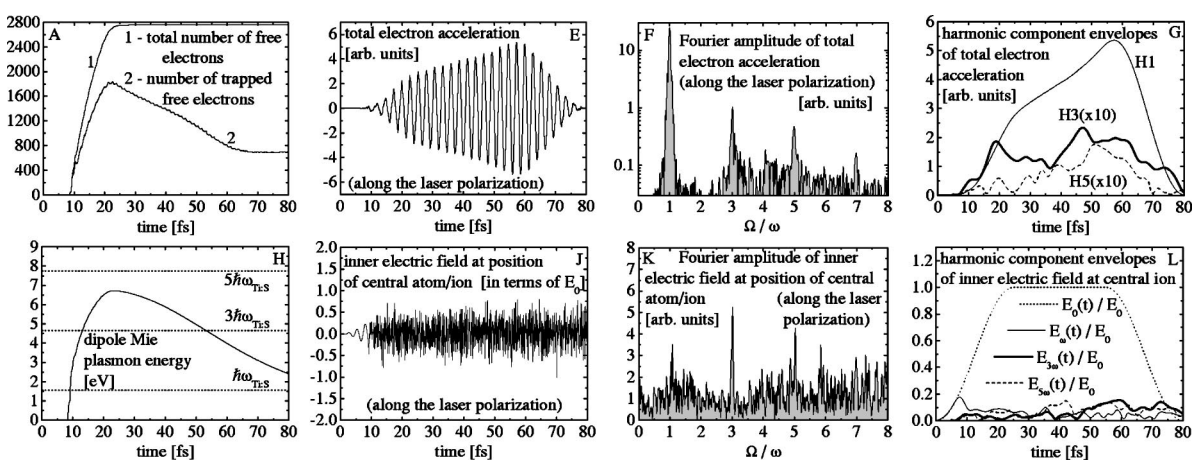

FIG. 7. As indicated on each panel, the panels show the nonlinear features of the laser-cluster interaction for a small (459 atoms) model xenon cluster with $Z_{\max} = 6$ exposed to a 80-fs laser pulse ($\lambda = 800$ nm, $I_0 = 4\times 10^{15}$ W/cm^2.

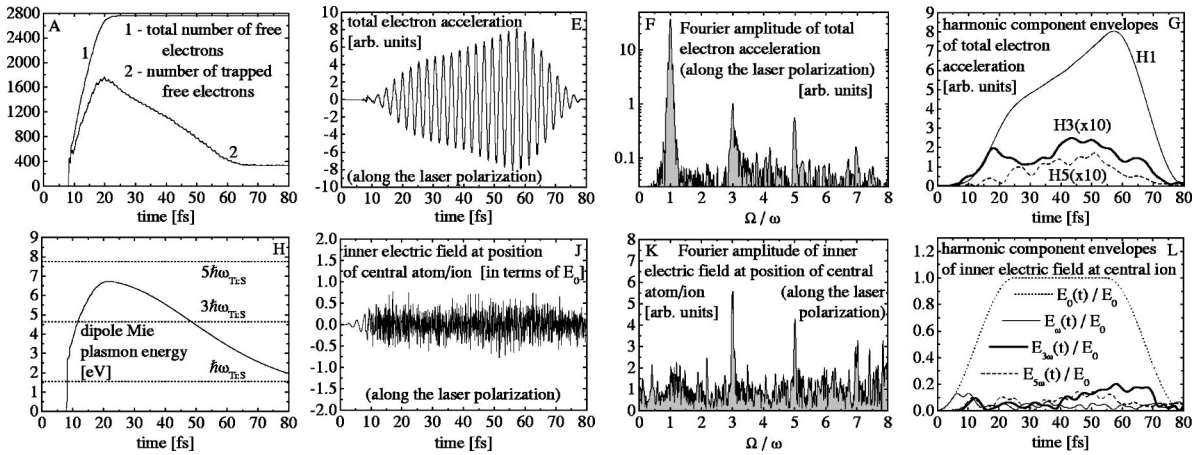

FIG. 8. Same as in Fig. 7, but for the higher laser intensity $I_0 = 6\times 10^{15}$ W/cm^2.

also becomes visible, especially in the xenon cluster [Figs. 7(F) and 8(F)]. As in the previous case of the two-electron atom, the third- and fifth-harmonic components of the inner electric field rise above a strong background of noise due to recombination of the electrons trapped inside the cluster. Again, this background is reduced with increasing laser intensity.

It is interesting that both for the argon and the xenon cluster the temporal behavior of the time-dependent Mie frequency [panels (H) of Figs. 5–8] is qualitatively very similar. Namely, for $\lambda = 800$ nm, the energy of five laser photons is slightly higher than the maximum value of the time-dependent nominal Mie-plasmon energy [calculated according to Eq. (1)], while the energy of three photons is notably lower. This appears to explain why in this case the energy of the fifth harmonic emitted during the laser pulse is of the same order as the third-harmonic energy. To investigate this in more detail, we consider the 675-atom argon cluster at the intensity of 4×10^{15} W/cm^2 and calculate the detunings from resonance $\Delta_n = n\hbar\omega - (\hbar\omega_{\mathrm{Mie}}(t))_{\max}$ for $n=3$ and $n=5$ [Fig. 9(A)] as a function of the laser wavelength and compare them with the energy emitted into the third and fifth harmonics [see the semilogarithmic plot of Fig. 9(B)]. As expected from the curves in Fig. 9(A), the third-harmonic energy rapidly decreases as the laser wavelength increases from 600 to 1000 nm, owing to the increasing value of $|\Delta_3(\lambda)|$ and the growing departure from the global resonance condition $\Delta_3(\lambda) = 0$.

It seems that this curve is the right-hand wing of a very pronounced resonance maximum located somewhat below 600 nm, so that the Ti:sapphire laser wavelength of 800 nm is off resonant. The evolution of the envelopes of the third harmonic of the total electron acceleration with decreasing laser wavelength [Fig. 9(C)] also supports this assumption. The width of the third-order resonance curve appears to be similar ($\sim$100 nm or $\sim$0.2 eV) to that obtained in the previous Sec. III A for the resonance curve of third-harmonic generation by the same cluster consisting of two-electron atoms. At the same time, in complete agreement with the behavior of $\Delta_5(\lambda)$, the energy emitted into the fifth harmonic exhibits resonance behavior, though less pronounced, with a maximum near $\lambda = 900$ nm. The fifth-order resonance is several times wider than the third-order resonance but still of the order of 1 eV. This value is still in agreement with the rate of electron-ion collisions, as mentioned in the previous subsection. However, the significance of collisions does increase for shorter wavelengths [41]. For $\lambda = 800$ nm, fifth-order har-

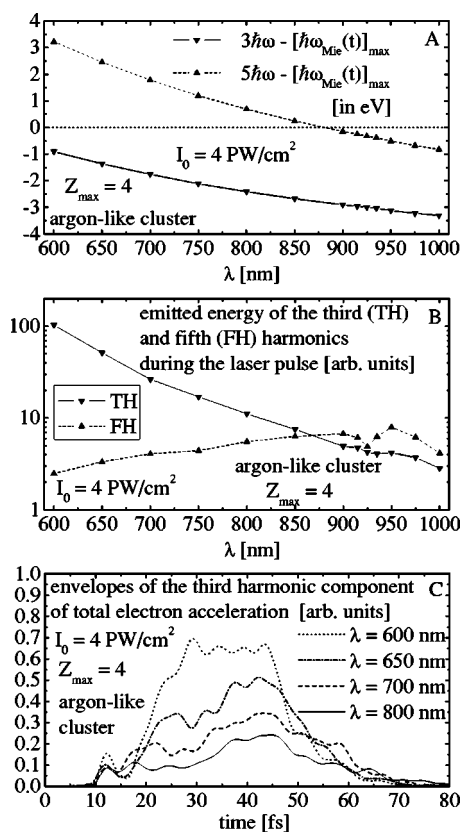

FIG. 9. Detuning (in eV) between 3 times and 5 times the energy of a laser photon and the maximal value of the time-dependent Mie-plasmon energy (1) versus the laser wavelength for the 675-atom argon model cluster with $Z_{\max} = 4$ at the laser intensity $I_0 = 4\times 10^{15}$ W/cm^2 [panel (A)], the resonance curves of the energies emitted into the third and fifth harmonics during the laser-pulse duration [panel (B)], and the time-dependent envelopes of the third harmonic of the total electron acceleration for four different wavelengths [panel (C)].

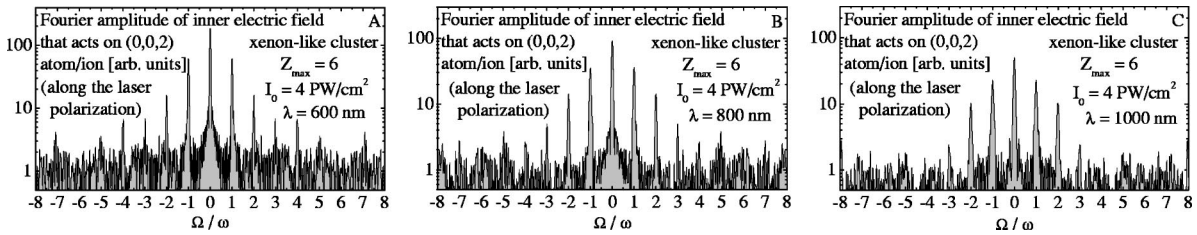

FIG. 10. For a small (459-atom) xenon cluster with $Z_{max}=6$, panels (A)–(C) show the Fourier-transform amplitudes of the inner-electric-field component along the laser polarization (the z axis of the fcc lattice) at the instantaneous positions of the noncentral (0, 0, 2) ion, for three laser wavelengths between 600 and 1000 nm and for the intensity $I_0=4\times10^{15}$ W/cm^2.

monic generation is almost on resonance and the emitted energy is comparable with the off-resonance generation of the third harmonic. The observed large difference in the widths of the third-order and the fifth-order resonance is an unexpected and interesting feature of the nonlinear electron dynamics in a laser-irradiated cluster. The actual fifth-order resonance position [cf. Fig. 9(B)] is redshifted with respect to the wavelength where $\Delta_5(\lambda)=0$ [Fig. 9(A)], as was the case for the third-order resonance in the two-electron-atom cluster. Moreover, as in the latter case [cf. Fig. 3(B)], we observe a "double-peak" structure of the resonance maximum, supporting the conclusion that this is a typical feature.

There is only one qualitative difference between argon (Figs. 5 and 6) clusters and xenon (Figs. 7 and 8) clusters, in so far as third-harmonic generation is concerned: for argon clusters, the third-harmonic envelope of the total electron acceleration [Figs. 5(G) and 6(G)] has only one pronounced maximum during the laser-pulse duration, while for xenon clusters, there are two [Figs. 7(G) and 8(G)]. This different behavior may be related to the fact that for the xenon cluster the Mie-plasmon energy as a function of time [Figs. 7(H) and 8(H)] rises more gently through the three-photon resonance than for the argon cluster [Figs. 5(H) and 6(H)], where this rise is abrupt, almost vertical. In analogy with the Landau-Zener level-crossing problem [51–53], we can conclude that at the time when the resonance condition $3\omega=\omega_{\mathrm{Mie}}(t)$ is met, the derivative $d(\hbar\omega_{\mathrm{Mie}}(t))/dt$ and the resonant Mie-plasmon excitation are inversely related. This explains that for the argon cluster the first maximum between 10 and 20 fs of the third-harmonic envelope of the total electron acceleration is hardly visible.

2. Second-harmonic excitation inside the cluster

As already shown in Sec. III A for a cluster consisting of 675 model argon atoms with $Z_{max}=2$ (Fig. 4), the second harmonic of the fundamental frequency is present in the Fourier transform of the inner electric field that acts on the (0, 0, 2) *moving* ion positioned off the cluster center. In this subsection, we concentrate on the properties of the second-harmonic excitation. For a 459-atom model xenon cluster with $Z_{max}=6$ and a laser intensity of 4×10^{15} W/cm^2, results of simulations are shown in Figs. 10 and 11.

Similarly to Fig. 4(B) of Sec. III A, Figs. 10(A)–10(C) exhibit the Fourier spectra along the laser polarization of the inner electric field that acts on the (0, 0, 2) noncentral ion, for three laser wavelengths in the range between 600 and 1000 nm. Here and in all subsequent calculations, the laser-field polarization is along the z axis of the fcc cluster lattice. We observe strong *nonresonant* excitation of the second harmonic for all laser wavelengths considered, with a magnitude comparable with the fundamental inside the cluster. We also observe a strong quasistatic component of the electric field, which is due to the cluster being charged as a consequence of outer ionization as well as to the noncentral position of the (0, 0, 2) ion. Comparison of Figs. 10(A)–10(C) also demonstrates that the inner field (all of its Fourier components) decreases with increasing wavelength. This indicates that the shielding of the incident field becomes more efficient for decreasing frequency (it was also checked that the number of trapped electrons at the end of the pulse increases with increasing wavelength), in spite of the increasing ponderomotive energy.

The presence of the second harmonic inside the cluster indicates efficient nonresonant two-photon excitation of the quadrupole [angular momentum $l=2$; cf. Eq. (2)] surface-plasmon oscillation [27]. To check this surmise, we examined the vector properties of the inner electric field that acts on three noncentral ions [(2, 0, 0), (0, 2, 0), and (0, 0, 2)] positioned on the three cubic axes of the cluster by calculating the Fourier spectrum of all three Cartesian components of the field. The results presented in Fig. 11(A)–11(I) show that the Fourier spectra of the x component of the inner electric field at the (2, 0, 0) ion [panel (A)] and of the y component at the (0, 2, 0) ion [panel (E)] are practically identical and display only the second-harmonic and quasistatic components. Similarly, the spectra of the z component at the (2, 0, 0) and (0, 2, 0) ions are identical with each other, but exhibit only odd harmonics [panels (C) and (F)]. Finally, the z component at the (0, 0, 2) ion [panel (I)] contains even as well as odd harmonics. The remaining field components [panels (B), (D), (G), and (H)] display no harmonics at all (only background noise).

Hence, in all cases the third-harmonic field is directed along the laser polarization only, confirming the dipole character of the third-harmonic excitation. On the other hand, the second-harmonic field at noncentral positions does have nonzero components in the direction of the respective radius vector. Such a field cannot be generated by oscillations of a rigid electron cloud without deformations. Similar results were obtained for other representative parameters.

The tensor character observed can be derived from a tensor decomposition of the susceptibility tensor in a straightforward fashion. To lowest order in the incident field $\mathbf{E}^{\mathrm{inc}}(\omega)$,

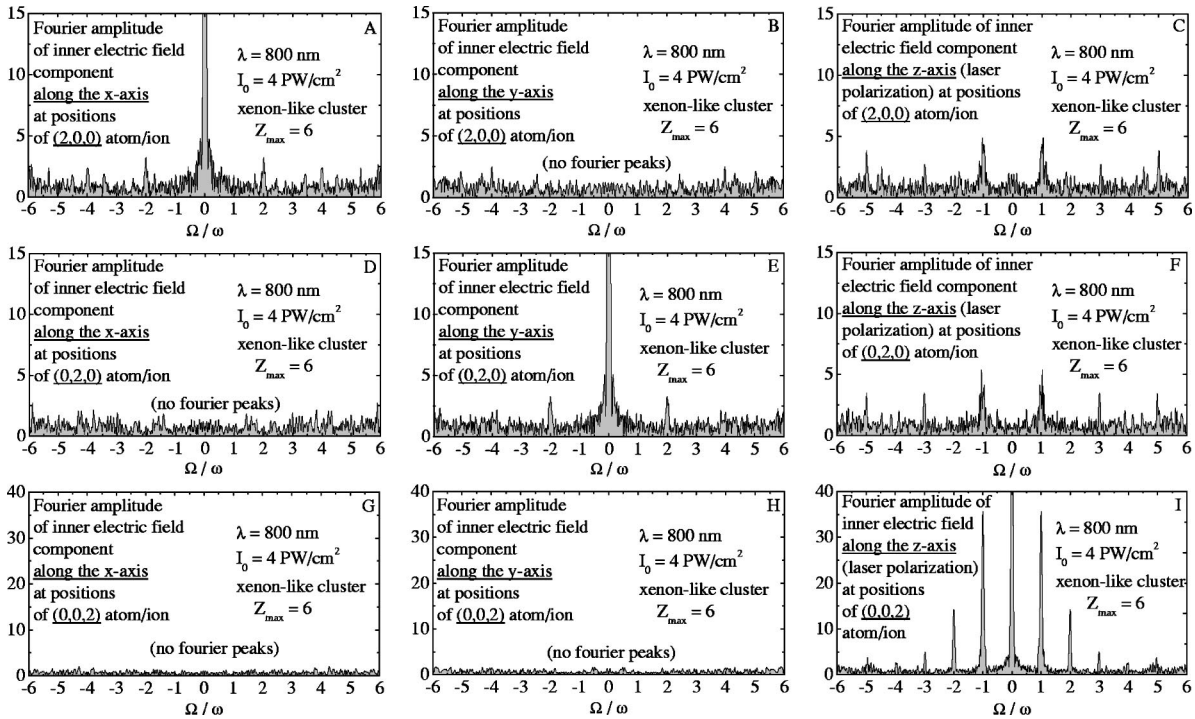

FIG. 11. For a small (459-atom) xenon cluster with $Z_{\max}=6$, panels (A)–(I) exhibit the Fourier-transform amplitudes of the inner-electric-field components in three orthogonal directions at the instantaneous positions of the noncentral ions (2, 0, 0) [panels (A)–(C)], (0, 2, 0) [panels (D)–(F)], and (0, 0, 2) [panels (G)–(I)]. The wavelength is $\lambda=800$ nm and the intensity $I_0=4\times10^{15}$ W/cm^2.

the second-harmonic quadrupole field at the position **r** inside the cluster is given by

$$E_i^{(2\omega)}(\mathbf{r}) = \chi_{ijk}^{(2)}(\mathbf{r})E_j^{\mathrm{inc}}(\omega)E_k^{\mathrm{inc}}(\omega), \tag{5}$$

where $\chi_{ijk}^{(2)}$ represents the second-order susceptibility tensor and summation over repeated indices is understood. In order to construct this tensor, the only building blocks available are the vector **r** and the Kronecker tensor δ_{ij}. Hence, for an isotropic cluster, the tensor structure of $\chi^{(2)}$ is restricted to

$$\chi_{ijk}^{(2)}(\mathbf{r}) = \alpha_2(r_i\delta_{jk} + r_j\delta_{ki} + r_k\delta_{ij}) + \beta_2 r_i r_j r_k, \tag{6}$$

where α_2 and β_2 depend on $\mathbf{r}^2$ and on the properties of the cluster in the absence of the field. For the third harmonic, the corresponding formulas are

$$E_i^{(3\omega)}(\mathbf{r}) = \chi_{ijkl}^{(3)}(\mathbf{r})E_j^{\mathrm{inc}}(\omega)E_k^{\mathrm{inc}}(\omega)E_l^{\mathrm{inc}}(\omega) \tag{7}$$

and

$$\chi_{ijkl}^{(3)}(\mathbf{r}) = \alpha_3(\delta_{ij}\delta_{kl} + \delta_{ik}\delta_{jl} + \delta_{il}\delta_{kj}) + \beta_3(r_i r_j \delta_{kl} + \text{permutations}) + \gamma_3 r_i r_j r_k r_l. \tag{8}$$

Equations (5)–(8) reproduce the vector properties of the second and third harmonics that are observed in Fig. 11 and have been summarized above. In particular, for the incident field $\mathbf{E}^{\mathrm{inc}}(\omega)\sim\hat{\mathbf{z}}$, Eqs. (5) and (6) reproduce the vector properties of the field $E_i^{(2\omega)}$ at the noncentral positions **r**. Allowing contributions of higher order in $\mathbf{E}^{\mathrm{inc}}$ in Eqs. (5) and (7), thereby defining χ's of higher order, does not change these conclusions. From the fact that Figs. 11(C) and 11(F) display a third harmonic at the off-center positions (2, 0, 0) and (0, 2, 0) we can immediately conclude that $\alpha_3\neq0$.

IV. CONCLUSION

This work was devoted to numerical simulations of the laser-cluster interaction with emphasis on the nonlinear collective electron dynamics and the generation of low-order harmonics in a comparatively small cluster consisting of $\lesssim10^3$ atoms. Our classical molecular-dynamics simulation model takes into account almost all of the ingredients of the laser-cluster interaction. In full qualitative agreement with the phenomenological picture of nonlinear oscillations of a cloud of electrons trapped inside a charged cluster in a strong laser field [28–30], we have observed a strong third-harmonic excitation when the tripled laser frequency is close to the Mie frequency—that is, near the third-order resonance with the Mie frequency. This corresponds to nonlinear excitation of the dipole surface plasmon. The resonant behavior can be seen both in the total electron acceleration (which is responsible for third-harmonic generation by the cluster) and in the internal electric field of the cluster (which is responsible for ionization of the cluster constituents). Varying the laser wavelength produces a pronounced resonance curve whose width affords an estimate of the width of the Mie resonance in a cluster irradiated by a strong laser field. The time-dependent envelopes of the total electron acceleration and of the inner electric field at the position of the central cluster ion have been calculated at the fundamental frequency and at the third harmonic. They display maxima at those times when the time-dependent Mie frequency (whose time dependence results from the time dependence of the mean charge density of the expanding ion core) satisfies the resonance condition.

Preliminary results of these simulations have already been presented in Ref. [46], where a cluster of two-electron model atoms was considered, with otherwise typical parameters. In the current paper, in addition to a more comprehensive study of the two-electron-atom cluster, we have extended our model to cluster atoms having more than two electrons. We allow sequential ionization of atoms and ions inside the cluster under the action of the inner electric field. This is much closer to the realistic case of rare-gas atomic clusters in a strong laser field, whose parameters for argon and xenon clusters were used in the calculations. We have confirmed the presence of the third harmonic (and of higher harmonics, especially the fifth) in the total electron acceleration as well as in the inner electric field at the position of the central ion and its resonant behavior when the frequency of the incident laser sweeps through the corresponding nonlinear resonance with the time-dependent Mie frequency. The dependence of the time-dependent yield of the third and fifth harmonics on the various parameters of the laser-cluster interaction was analyzed. Moreover, we have observed a strong presence of the second harmonic in the local electric field acting on noncentral ions. The vector character of this second harmonic as observed in the simulation allowed us to attribute it to nonresonant excitation of the quadrupole surface plasmon.

Finally, we should mention that the insensitivity of the results presented in this paper with respect to the ion configuration, ionization model, and propagation method was checked against a completely independent molecular-dynamics computer code. In this latter much more time-consuming code, all active electrons were present from the beginning, undergoing bound motion in the parent ion potential up to the time when inner ionization occurs. A simple cubic ion structure was used which yields the numerical benefit of an exact fourfold symmetry if the orientation of the polarization axis of the laser field is properly chosen. The conclusion is that harmonic generation in clusters is a robust phenomenon, which is largely independent of the details of the model of the cluster and the computational procedures.

ACKNOWLEDGMENTS

The authors are very grateful to Jan-Michael Rost and Ulf Saalmann for fruitful discussions. This work was supported by the Deutsche Forschungsgemeinschaft [Project No. 436 RUS 113/676/0-1(R)] and by the Russian Foundation for Basic Research (Grant Nos. 02-02-04007NNIO-a and 03-02-17112). D.B. gratefully acknowledges support by the Heisenberg program.

[1] T. Ditmire, T. Donnelly, A. M. Rubenchik, R. W. Falcone, and M. D. Perry, Phys. Rev. A **53**, 3379 (1996).
[2] T. Ditmire, R. A. Smith, J. W. G. Tisch, and M. H. R. Hutchinson, Phys. Rev. Lett. **78**, 3121 (1997).
[3] T. Ditmire, E. Springate, J. W. G. Tisch, Y. L. Shao, M. B. Mason, N. Hay, J. P. Marangos, and M. H. R. Hutchinson, Phys. Rev. A **57**, 369 (1998).
[4] A. McPherson, B. D. Thompson, A. B. Borisov, K. Boyer, and C. K. Rhodes, Nature (London) **370**, 631 (1994).
[5] A. McPherson, T. S. Luk, B. D. Thompson, A. B. Borisov, O. B. Shiryaev, X. Chen, K. Boyer, and C. K. Rhodes, Phys. Rev. Lett. **72**, 1810 (1994).
[6] T. Ditmire, T. Donnelly, R. W. Falcone, and M. D. Perry, Phys. Rev. Lett. **75**, 3122 (1995).
[7] M. Schnürer, S. Ter-Avetisyan, H. Stiel, U. Vogt, W. Radloff, M. Kalashnikov, W. Sandner, and P. V. Nickles, Eur. Phys. J. D **14**, 331 (2001).
[8] S. Ter-Avetisyan, M. Schnürer, H. Stiel, U. Vogt, W. Radloff, W. Karpov, W. Sandner, and P. V. Nickles, Phys. Rev. E **64**, 036404 (2001).
[9] E. M. Snyder, S. A. Buzza, and A. W. Castleman, Jr., Phys. Rev. Lett. **77**, 3347 (1996).
[10] T. Ditmire, J. W. G. Tisch, E. Springate, M. B. Mason, N. Hay, R. A. Smith, J. Marangos, and M. H. R. Hutchinson, Nature (London) **386**, 54 (1997).
[11] M. Lezius, S. Dobosz, D. Normand, and M. Schmidt, Phys. Rev. Lett. **80**, 261 (1998).
[12] T. Ditmire, J. Zweiback, V. P. Yanovsky, T. E. Cowan, G. Hays, and K. B. Wharton, Nature (London) **398**, 489 (1999).
[13] J. Zweiback, R. A. Smith, V. P. Yanovsky, T. E. Cowan, G. Hays, K. B. Wharton, and T. Ditmire, in *Multiphoton Processes*, edited by L. F. DiMauro, R. R. Freeman, and K. C. Kulander, AIP Conf. Proc. No. 525 (AIP, Melville, NY, 2000), pp. 534–543.
[14] T. D. Donnelly, T. Ditmire, K. Neuman, M. D. Perry, and R. W. Falcone, Phys. Rev. Lett. **76**, 2472 (1996).
[15] J. W. G. Tisch, T. Ditmire, D. J. Fraser, N. Hay, M. B. Mason, E. Springate, J. P. Marangos, and M. H. R. Hutchinson, J. Phys. B **30**, L709 (1997).
[16] *Molecules and Clusters in Intense Laser Fields*, edited by Jan Posthumus (Cambridge University Press, Cambridge, England 2001).
[17] F. Calvayrac, P.-G. Reinhard, E. Suraud, and C. A. Ullrich, Phys. Rep. **337**, 493 (2000).
[18] V. P. Krainov and M. B. Smirnov, Phys. Rep. **370**, 237 (2002).
[19] G. Mie, Ann. Phys. (Leipzig) **25**, 377 (1908).
[20] M. Ya. Amusia and J.-P. Connerade, Rep. Prog. Phys. **63**, 41 (2000).
[21] C. A. Ullrich, P.-G. Reinhardt, and E. Suraud, J. Phys. B **30**, 5043 (1997).
[22] P.-G. Reinhardt and E. Suraud, Eur. Phys. J. D **3**, 175 (1998).
[23] L. Köller, M. Schumacher, J. Köhn, S. Teuber, J. Tiggesbäumker, and K. H. Meiwes-Broer, Phys. Rev. Lett. **82**, 3783 (1999).
[24] *Physical Quantities Handbook*, edited by I. S. Grigoryev and E. S. Meilikhov (Energoatomizdat, Moscow, 1991) (in Russian).
[25] S. Augst, D. Strickland, D. D. Meyerhofer, S. L. Chin, and J. H. Eberly, Phys. Rev. Lett. **63**, 2212 (1989).
[26] A. A. Radzig and B. M. Smirnov, *Reference Data on Atoms, Molecules and Ions* (Springer, Berlin, 1985).
[27] J.-P. Connerade and A. V. Solov'yov, Phys. Rev. A **66**, 013207

(2002).
[28] S. V. Fomichev, S. V. Popruzhenko, D. F. Zaretsky, and W. Becker, J. Phys. B **36**, 3817 (2003).
[29] S. V. Fomichev, S. V. Popruzhenko, D. F. Zaretsky, and W. Becker, Opt. Express **11**, 2433 (2003).
[30] S. V. Fomichev, S. V. Popruzhenko, and D. F. Zaretsky, Laser Phys. **13**, 1188 (2003).
[31] K. Hagino, Phys. Rev. B **60**, R2197 (1999).
[32] L. G. Gerchikov, C. Guet, and A. N. Ipatov, Phys. Rev. A **66**, 053202 (2002).
[33] G. Hays, B. Shim, M. C. Downer, and T. Ditmire (unpublished).
[34] M. Fomyts'kyi, B. Breizman, A. Arefiev, and C. Chiu (unpublished).
[35] M. Fomyts'kyi, B. Breizman, A. Arefiev, and C. Chiu, Phys. Plasmas **11**, 3349 (2004).
[36] C. Jungreuthmayer, M. Geissler, J. Zanghellini, and T. Brabec, Phys. Rev. Lett. **92**, 133401 (2004).
[37] T. Ditmire, Phys. Rev. A **57**, R4094 (1998).
[38] I. Last and J. Jortner, Phys. Rev. A **60**, 2215 (1999).
[39] I. Last and J. Jortner, Phys. Rev. A **62**, 013201 (2000).
[40] K. Ishikawa and T. Blenski, Phys. Rev. A **62**, 063204 (2000).
[41] D. Bauer, J. Phys. B **37**, 3085 (2004).
[42] T. Döppner, S. Teuber, M. Schumacher, J. Tiggesbäumker, and K. H. Meiwes-Broer, Appl. Phys. B: Lasers Opt. **71**, 357 (2000).
[43] C. Siedschlag and J. M. Rost, Phys. Rev. Lett. **89**, 173401 (2002).
[44] C. Siedschlag and J. M. Rost, Phys. Rev. A **67**, 013404 (2003).
[45] U. Saalmann and J.-M. Rost, Phys. Rev. Lett. **91**, 223401 (2003).
[46] S. V. Fomichev, D. F. Zaretsky, and W. Becker, J. Phys. B **37**, L175 (2004).
[47] C. Rose-Petruck, K. J. Schafer, K. R. Wilson, and C. P. J. Barty, Phys. Rev. A **55**, 1182 (1997).
[48] D. Bauer and A. Macchi, Phys. Rev. A **68**, 033201 (2003).
[49] M. R. Hoare, Adv. Chem. Phys. **40**, 49 (1979).
[50] D. W. Heermann, *Computer Simulation Methods in Theoretical Physics*, 2nd ed. (Springer-Verlag, Berlin, 1990).
[51] L. D. Landau, Phys. Z. Sowjetunion **1**, 88 (1932).
[52] L. D. Landau, Phys. Z. Sowjetunion **2**, 46 (1932).
[53] C. Zener, Proc. R. Soc. London, Ser. A **137**, 696 (1932).
[54] K.-A. Suominen, Opt. Commun. **93**, 126 (1992).
[55] V. Kresin, Phys. Rev. B **39**, 3042 (1989).
[56] V. Kresin, Phys. Rep. **220**, 1 (1992).
[57] E. M. Lifshits and L. P. Pitaevsky, *Physical Kinetics* (Pergamon, Oxford, 1981).
[58] F. Brunel, Phys. Rev. Lett. **59**, 52 (1987).
[59] F. Brunel, Phys. Fluids **31**, 2714 (1988).